narra j

Original Article

Plant-based synthesis of gold and silver nanoparticles using *Artocarpus heterophyllus* aqueous leaf extract and its anticancer activities

Firli RP. Dewi[1,2*], Aulia U. Rohmatika[1], Arniza KM. Jamil[3], Turan Demircan[4], Muhammad F. Idris[1], Litazkiyyah Litazkiyyah[1], Muhammad Fahmi[1], A'liyatur Rosyidah[5], Alfiah Hayati[1] and Sugiharto Sugiharto[1]

[1]Department of Biology, Faculty of Science and Technology, Universitas Airlangga, Surabaya, Indonesia; [2]Research Center for Stem Cells Development, Universitas Airlangga, Surabaya, Indonesia; [3]Department of Chemistry, Faculty of Science, Universiti Malaya, Kuala Lumpur, Malaysia; [4]Department of Medical Biology, School of Medicine, Muğla Sıtkı Koçman University, Muğla, Turkey; [5]Research Center for Vaccine and Drugs, National Research and Innovation Agency (BRIN), Bogor, Indonesia

*Corresponding author: firli.rahmah@fst.unair.ac.id

Abstract

Green synthesis of nanoparticles has garnered significant attention for its sustainable and environmentally friendly approach. Despite extensive research on *Artocarpus heterophyllus*-derived nanoparticles using seeds, fruits, and rind, the therapeutic potential of its leaf extract remains largely unexplored, particularly in MCF-7 breast cancer cells. The aim of this study was to investigate the potential of aqueous leaf extract from *A. heterophyllus* as a reducing and capping agent to synthesize silver nanoparticles (AgNPs) and gold nanoparticles (AuNPs), as well as to evaluate their anticancer efficacy. The nanoparticles were characterized using ultraviolet-visible spectroscopy, transmission electron microscopy, Fourier-transform infrared spectroscopy, X-ray diffraction, and particle size analysis to confirm the formation. To evaluate anticancer potential, key oncogenes associated with cancer proliferation and survival were analyzed, including *c-Myc*, *cyclin D1*, *human epidermal growth factor receptor-2 (HER-2)*, *microRNA-622* (*miR-622*), and *cyclooxygenase-2 (COX-2)*. The present study demonstrated that AgNPs and AuNPs synthesized from *A. heterophyllus* extract had distinct sizes and shapes, with AgNPs averaging approximately 12.75 nm and exhibiting a spherical morphology, while AuNPs averaged 109.26 nm and had a pentagonal shape. Furthermore, AuNPs had no anticancer activity. In contrast, AgNPs showed potent anticancer effects, with inhibitory concentration (IC_{50}) values of 124.626 and 54.981 µg/mL at 48 and 72 hours, respectively. The AgNPs treatment increased the proportion of cells in G2/M phase, indicating the induction of mitotic catastrophe leading to cell death. AgNPs downregulated the expression of several oncogenes associated with cancer cell proliferation and survival (*cyclin D1, COX-2, HER-2*, and *miR622),* but did not significantly reduce *c-Myc* expression. In conclusion, AgNPs derived from *A. heterophyllus* leaf extract have significant potential as a novel therapeutic agent in cancer treatment while preserving its biocompatibility, emphasizing the promise of sustainable and cost-effective synthesis of plant-based nanoparticles.

Keywords: Breast cancer, *A. heterophyllus*, nanoparticles, green synthesis, mitotic

Introduction

The pursuit of innovative and effective treatments for breast cancer remains a critical focus in medical research, owing to the disease's high incidence and mortality rate [1-3]. Recent

https://narraj.org/

Received: November 13, 2024 - Accepted: April 6, 2025 - Published online: April 27, 2025

advancements in nanotechnology have emerged as a promising strategy for enhancing cancer therapies, particularly through its potential for targeted drug delivery [4]. This expansive field involves the manipulation of materials at the nanoscale to induce novel properties and functionalities [4]. Within this field, nanomedicine represents a specialized subset of nanotechnology that applies manipulation of materials principles to the medical field, including the diagnosis, treatment, and prevention of diseases [7]. Among the diverse array of nanomaterials, metallic nanoparticles—specifically silver nanoparticles (AgNPs) and gold nanoparticles (AuNPs)—have garnered significant attention due to their exceptional physicochemical properties, biocompatibility, and ability to interact with biological systems at the molecular level [5-7].

Numerous studies have highlighted the broad potential of AgNPs and AuNPs across various applications, including antimicrobial, anticancer, anti-proliferative, anti-inflammatory, antibacterial, and antiangiogenic effects [8-12]. These nanoparticles also possess robust antioxidant properties, as demonstrated by the 1,1-diphenyl-2-picrylhydrazyl (DPPH) assay [12]. Moreover, AgNPs and AuNPs have proven effective as catalysts for the reduction of organic dyes [12]. Given these promising attributes, the method of synthesis employed for AgNPs and AuNPs plays a critical role in determining efficacy and potential applications. Although traditional physical and chemical synthesis methods are effective, these approaches often involve toxic reagents and harsh conditions, which may compromise biocompatibility and environmental safety of the resulting nanoparticles [13,14].

Green synthesis methods, particularly those utilizing plant extracts, have garnered significant interest for producing nanoparticles in a sustainable and environmentally friendly manner [5,15,16]. This eco-friendly approach not only enhances the biocompatibility of nanoparticles but also aligns with sustainable development principles, positioning it as a promising alternative for large-scale production of AgNPs and AuNPs with diverse biomedical and industrial applications [17]. Plant-based synthesis exploits natural sources as reducing, capping, and stabilizing agents, including polyphenols, flavonoids, alkaloids, tannins, saponins, and terpenoids, which influence the size, shape, and functionality of nanoparticles [17,18]. Additionally, this method is cost-effective and reduces toxicity to normal cells, further highlighting its potential in nanoparticle production [19].

Artocarpus heterophyllus, commonly known as jackfruit, has emerged as a prominent natural source for medicinal applications [20]. Extracts derived from its wood, seeds, and flowers have demonstrated promising anticancer activities against various cancer cell lines, including Caco-2, HCT116, WiDr, H460, and MCF-7 [20-22]. Additionally, crude extracts from *A. heterophyllus* wood pulp have shown anti-inflammatory and chemopreventive properties in HCT116 cells [21]. The synthesis of AgNPs and AuNPs using *A. heterophyllus* typically involved its seeds, fruits, and rind [23-25]; however, the potential of its leaves remains underexplored, particularly regarding effects on MCF-7 cells as a model for human breast cancer. The aim of this study was to conduct green synthesis of AgNPs and AuNPs using *A. heterophyllus* leaf extract and to assess the potential of these nanoparticles as anti-breast cancer agents by evaluating their ability to inhibit cell viability and influence breast cancer signaling pathways.

Methods

Study design and setting

An experimental study was conducted in the Laboratory of Molecular Genetics, Universitas Airlangga, Surabaya, Indonesia, in collaboration with the Department of Chemistry, University of Malaya, Kuala Lumpur, Malaysia, to explore the potential of *A. heterophyllus* aqueous leaf extract as a reducing and capping agent in the synthesis of AgNPs and AuNPs. The synthesis process was optimized by controlling key parameters, including pH, temperature, and extract concentration, to ensure the stability and efficacy of the nanoparticles. Comprehensive characterization was performed using ultraviolet-visible (UV-Vis) spectroscopy to confirm nanoparticle formation, transmission electron microscopy (TEM) to determine morphology, Fourier transform infrared spectroscopy (FT-IR) to identify functional groups involved in capping, X-ray diffraction (XRD) to assess crystallinity, and particle size analysis (PSA) to

evaluate size distribution. To assess anticancer potential, molecular biology techniques were employed, focusing on the expression of key oncogenes associated with cancer cell proliferation and survival, including *c-Myc*, *cyclin D1*, *human epidermal growth factor receptor-2 (HER-2)*, *microRNA-622* (*miR-622*), and *cyclooxygenase-2 (COX-2)*.

Preparation of *Artocarpus heterophyllus* leaf extract

To prepare the aqueous extract of *A. heterophyllus*, fresh leaves were obtained from the Faculty of Science and Technology, Universitas Airlangga, Surabaya, Indonesia. Ten grams of leaves were thoroughly washed under running water, followed by rinsing with deionized water to remove any residual contaminants. The cleaned leaves were finely diced and immersed in 100 mL of double-distilled water (ddH_2O) at pH 7.0. The mixture was continuously stirred and heated at 60°C for 40 minutes using an RT2 advanced hotplate stirrer (Thermo Fisher Scientific, Waltham, MA, USA) to facilitate the extraction of bioactive compounds. After heating, the extract was allowed to cool to room temperature (10–15 minutes) before being filtered through a 0.22 µm MF-Millipore membrane to remove particulates. The final volume of the extract was approximately 95 mL, which was either used immediately for further experiments or stored at 4°C in sterile, airtight containers to prevent contamination and preserve the stability of active phytochemicals.

Synthesis of silver nanoparticles (AgNPs) and gold nanoparticles (AuNPs)

The biosynthesis of AgNPs was conducted by mixing 50 mL of *A. heterophyllus* aqueous leaf extract with 50 mL of 0.1 M silver nitrate 100% purity ($AgNO_3$) (Merck, Darmstadt, Germany). The solution's pH was adjusted to 7.0 using 0.1 M NaOH (MilliporeSigma, Massachusetts, MA, USA; 99.99% purity). The mixture was incubated at room temperature in the dark for 24 hours without stirring. A color change from beige to dark brown indicated the reduction of silver ions and nanoparticle formation. The synthesized AgNPs were freeze-dried for 24 hours and stored at 1–4°C. The final yield after freeze-drying was 0.138 g.

A gold ion solution was prepared by dissolving 50 mg of hydrogen tetrachloroaurate ($HAuCl_4$) (Smart Lab, Jakarta, Indonesia) in 50 mL of deionized water, yielding a 1 g/L solution. For AuNP synthesis, 50 mL of this gold ion solution was mixed with 50 mL of *A. heterophyllus* aqueous leaf extract. The mixture was incubated at room temperature in the dark for 24 hours without stirring. A color change to purple indicated the reduction of gold ions and the formation of AuNPs. The resulting AuNPs were freeze-dried for 24–48 hours and stored at 1–4°C. The final yield after freeze-drying was 0.141 g.

Characterization of AgNPs and AuNPs

The formation of AgNPs and AuNPs was verified using UV-Vis spectroscopy (Thermo Fisher Scientific, Waltham, MA, USA), conducted at 2 nm intervals within the range of 300–700 nm. Absorbance values were recorded to indicate the surface plasmon resonance peaks of the nanoparticles. Functional groups involved in the bioreduction reaction were analyzed using a Spectrum 100 FT-IR spectrometer (Perkin Elmer, Utah, USA) using the attenuated total reflectance (ATR) mode, covering a wavelength range of 4000 to 400 cm^{-1}. The results were presented as transmittance curves.

Particle size distribution in the liquid phase was determined using a PSA (Biobase BK-802N, Shandong, China). The refractive index and viscosity of the test samples were first analyzed to assess nanoparticle properties, such as chemical reactivity, stability, and biocompatibility. Briefly, 2 mL sample was then introduced into the PSA cuvette, where a laser beam was directed into the sample, and the intensity of the reflected light was measured to determine particle size and distribution. The results were presented as size distribution curves, indicating the size with the highest percentage.

Morphological analysis was conducted using transmission electron microscopy FEI Tecnai G2 F20 X-TWIN (FEI Company, Eindhoven, Netherlands). A small number of nanoparticles was placed on a copper grid, dried under ambient conditions, and observed under TEM. Images were captured from the electron flux after it passed through a thin sample of nanoparticles. The crystallinity of the biologically produced nanoparticles was examined using a PANalytical Empyrean X-ray diffractometer (EA Almelo, Almelo, Netherlands). Prior to XRD analysis, the nanoparticles were freeze-dried using a Lyovapor L-200 (BUCHI, Flawil, Switzerland) at

temperatures ranging from -55°C to -57°C under a pressure of 2 mbar for 24–48 hours. The XRD pattern of the freeze-dried nanoparticles was scanned using Cu Kα radiation in the 2θ range of 5° to 80°. All characterization analyses were performed in duplicate.

Cell proliferation analysis and inhibitory concentration (IC_{50}) determination

The anticancer effectiveness of the nanoparticles was evaluated using a 3-(4,5-dimethylthiazol-2-yl)-2,5-diphenyltetrazolium bromide (MTT) assay. A total of 5 mg of MTT powder (Invitrogen, Thermo Fisher Scientific, Waltham, MA, USA) was mixed with 1 mL of phosphate-buffered saline (PBS). The mixture was vortexed, filtered through a 0.22 µm syringe filter. MCF-7 cells (obtained from the Stem Cell Research and Development Center, Universitas Airlangga, Surabaya, Indonesia) were plated at a density of 5,000 cells per well in a 96-well plate with Dulbecco's modified Eagle's medium (DMEM) (Gibco, Thermo Fisher Scientific, Waltham, MA, USA). After 24 hours of incubation at 37°C with 5% CO_2, the cells were exposed to normal freshwater (control), doxorubicin at 10 µg/mL (positive control), or various concentrations of AgNPs and AuNPs (0, 12.5, 25, 50, 100, and 200 µg/mL) for 24, 48, and 72 hours. MTT solution (5 mg/mL) was added to each well, and the plates were incubated at 37°C for 4 hours. After medium removal, 100 µL of dimethyl sulfoxide (DMSO) was added to dissolve the formazan crystals. The plate was shaken for 15 minutes, and optical density (OD) was measured at 570 nm using a microplate reader (Bio-Rad, California, USA). To calculate cell viability, OD values from treated wells were normalized against control wells (untreated cells), representing 100% viability. The OD of the medium (containing nanoparticles) was subtracted from all measurements to eliminate non-specific absorbance. All measurements were performed in triplicate, and mean values were used to ensure precision and reliable comparisons between the treated and control groups. The IC_{50} value was determined using GraphPad Prism 8 (GraphPad Software, Boston, USA) based on the OD values obtained from the MTT assay results.

Cell cycle and DNA content analysis

The DNA content of MCF-7 cells was measured using 4′,6-diamidino-2-phenylindole (DAPI) staining. Cells were fixed with 4% paraformaldehyde and stained with 1 µg/mL DAPI C001 (ABP Biosciences, Beltsville, MD, USA) for 20 minutes at room temperature in the dark to evaluate distribution across cell cycle phases, followed by three washes with PBS. The cells were visualized and analyzed using the Cell-Insight CX7 Pro High Content Screening (HCS) System (Thermo Fisher Scientific, Waltham, MA, USA). The imaging settings were as follows: autofocus interval set to 2, camera model PRIMEBSI 1.53, and objective lens with 20× magnification. Analysis was performed using Thermo Scientific HCS Studio 5.0 Cell Analysis Software (Thermo Fisher Scientific, Waltham, MA, USA). Cells with DNA content 2N indicated the G1 phase, DNA content 2N-4N indicated the S phase, and DNA content 4N indicated the G2/M phase.

RNA isolation and gene expression analysis

MCF-7 cells were cultured in 6-well plates and divided into four groups for a 48-hour treatment period: the control group (treated with DMSO), positive control group (treated with doxorubicin at 10 µg/mL), and AgNP group (treated with AgNPs at 100 µg/mL). Total RNA was isolated using the Total RNA Mini Kit (Geneaid, New Taipei City, Taiwan) according to the manufacturer's instructions. RNA purity and concentration were measured using a µDrop plate integrated with SkanIt software v7.1 (Thermo Fisher Scientific, Waltham, MA, USA), with absorbances at 230, 260, and 280 nm. cDNA synthesis was performed using ReverTra Ace qPCR RT Master Mix (Toyobo, Osaka, Japan) following the provided protocol (reaction temperatures: 37°C for 15 minutes, 50°C for 5 minutes, and 98°C for 5 minutes). Quantitative PCR (qPCR) was carried out using Thunderbird Next SYBR qPCR Mix (Toyobo, Osaka, Japan) under the following conditions: predenaturation at 95°C for 60 seconds, followed by 40 cycles of denaturation at 95°C for 5 seconds and annealing/extension at 60°C for 30 seconds. qPCR reactions, with specific primers for the target genes (**Table 1**), were conducted in a 20 µL reaction volume. Forward and reverse primers (0.3 µM) for *c-Myc, cyclin D1, HER-2, miR622, COX-2*, and *GAPDH* were obtained from previous studies [26-30]. *GAPDH* served as the internal control or reference gene.

The threshold value was determined automatically using the MyGo Pro application (IT-IS International, UK). Gene expression analysis was performed using the relative quantification

method, and the reliability of the qPCR results was verified through melting curve analysis. The fold change in mRNA expression was calculated using the formula: $2^{(-[(Ctg - Cct) - average\ of\ Cct])}$, where Ct represents the cycle threshold, tg refers to the target gene, and ct indicates the control gene.

Table 1. Primers used for the target genes

Genes	Forward primer	Reverse primer
c-Myc	5'-GGAGGAACAAGAAGATGAGG-3'	5'-GTAGTTGTGCTGATGTGTGG-3'
cyclin D1	5'-AACTACCTGGACCGCTTCCT-3'	5'-CCACTTGAGCTTGTTCACCA-3'
HER2	5'-CCGAGGGCCGGTATACATTC-3'	5'-GCTTGCTGCACTTCTCACAC-3'
miR622	5'-GGGTCCGAGGTATTCGCACT-3'	5'-GCACAGTCTGCTGAGGTTGGA-3'
COX2	5'-CCGGGTACAATCGCACTTAT-3'	5'-GGCGCTCAGCCATACAG-3'
GAPDH	5'-GTCAGTGGTGGACCTGACCT-3'	5'-AGGGGTCTACATGGCAACTG-3'

Statistical analysis

Statistical analyses were performed using GraphPad Prism version 8 (GraphPad Software, Boston, USA). Data normality was assessed using the Shapiro–Wilk test. One-way analysis of variance (ANOVA) was employed to evaluate differences among experimental groups. When the ANOVA yielded a significant $p<0.050$, Tukey's honestly significant difference (HSD) post hoc test was applied to determine intergroup differences. Data are expressed as mean±standard deviation (SD), and $p<0.050$ were considered statistically significant.

Results

Characteristics of AgNPs from *Artocarpus heterophyllus* aqueous leaf extract

In the study, a noticeable color shift from beige to dark brown was observed (**Figure 1A**), and a prominent plasmon resonance peak was detected in the 420–440 nm range in the UV-Vis absorption spectra of AgNPs synthesized with *A. heterophyllus* aqueous leaf extract (**Figure 1B**). This peak confirmed the successful formation of AgNPs, as the leaf extract itself showed no peaks in the 300–600 nm range (**Figure 1B**). These results suggest the accomplishment of the reduction process carried out by *A. heterophyllus* aqueous leaf extract.

Further analysis of the size, shape, and crystal structure of the green-synthesized AgNPs was performed using TEM and PSA. AgNPs were predominantly spherical, with sizes ranging from 5 to 22 nm and an average diameter of 12.75 nm (**Figures 1C** and **1D**). The TEM images also confirmed the effective capping ability of the *A. heterophyllus* aqueous leaf extract (**Figure 1C**). Additionally, the XRD patterns of the synthesized AgNPs had small, broad peaks at 38.29°, 44.37°, 64.64°, and 77.50°, corresponding to the (111), (200), (220), and (311) crystallographic planes (**Figure 1E**). These findings indicated that the nanoparticles possessed a surface-centered cubic structure.

Characteristics of AuNPs from *Artocarpus heterophyllus* aqueous leaf extract

The successful formation of AuNPs was indicated by the distinct purple color that emerged when the *A. heterophyllus* aqueous leaf extract solution was combined with the $HAuCl_4$ solution (**Figure 2A**). During the synthesis, the plant extract acted as a potent reducing agent, converting Au^{3+} ions into Au^0. The resulting colloidal solutions were analyzed using UV-Vis spectroscopy, which revealed an absorption peak around 550 nm (**Figure 2B**). This peak aligned with the surface plasmon resonance characteristic of AuNPs, typically observed between 500 and 600 nm, depending on their size and shape [31]. To further examine the morphology of the AuNPs, TEM imaging was performed, revealing polygonal and hexagonal structures (**Figure 2C**). The particle size distribution, determined by PSA, showed an average particle size of 109.26 nm with a range from 27 to 201 nm (**Figure 2D**). The crystalline nature of the biologically synthesized AuNPs was confirmed through XRD (**Figure 2E**). The obtained XRD peaks at 2θ angles of 38.37°, 44.58°, 64.85°, and 77.83° corresponded to the (111), (200), (220), and (311) crystalline gold planes of a face-centered cubic structure, respectively.

Fourier transform infrared (FT-IR) spectroscopic analysis of functional groups in *Artocarpus heterophyllus*-mediated nanoparticle synthesis

FT-IR spectroscopy was performed to identify the functional groups present in both *A. heterophyllus* aqueous leaf extract and the synthesized nanoparticles. The FT-IR spectra of the

A. heterophyllus aqueous leaf and nanoparticles had notable similarities (**Figure 3**). The characteristic C-H aromatic stretching at 2,925 cm^{-1} and O-H vibrations from the phenol group at 3,300 cm^{-1} were observed in both the *A. heterophyllus* aqueous leaf and nanoparticles. Additionally, the prominent absorption band at 1,584 cm^{-1} in the extract, attributed to C=C stretching of the aromatic ring, shifted to 1,604 cm^{-1} with reduced intensity in both AuNPs and AgNPs. These spectral changes, including peak shifts and intensity variations, suggest an interaction between the bioactive compounds in *A. heterophyllus* aqueous leaf and the metal precursors. This interaction likely played a crucial role in the bioreduction of silver and gold ions, leading to the formation of AgNPs and AuNPs, respectively.

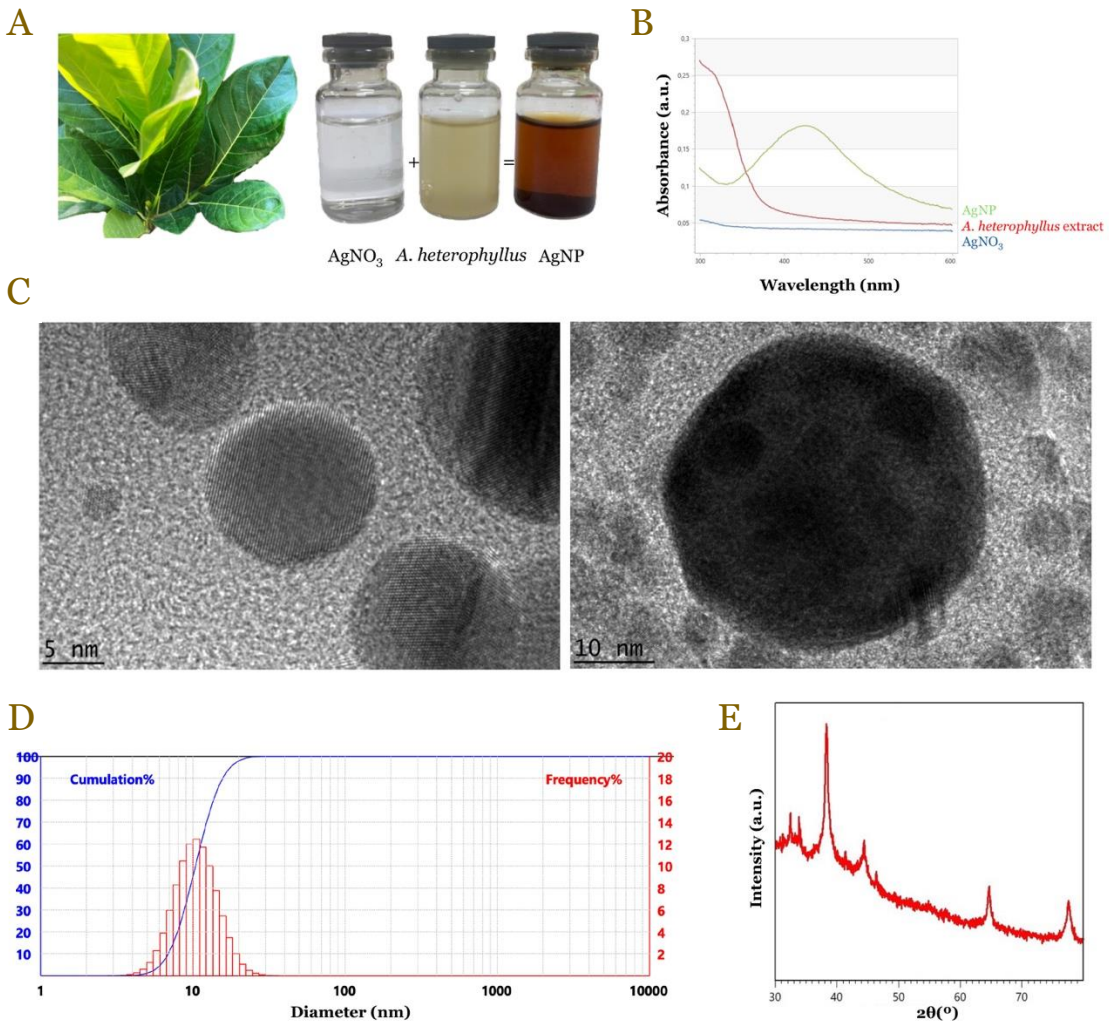

Figure 1. Synthesis and characterization of silver nanoparticles (AgNPs) using *Artocarpus heterophyllus* aqueous leaf extract. (A) The observed color changes during AgNP synthesis; (B) ultraviolet-visible (UV-Vis) spectrophotometric analysis of the synthesized AgNPs; (C) transmission electron microscopy (TEM) images detailing AgNP morphology; (D) particle size analysis (PSA) results representing AgNP size distribution; (E) X-ray diffraction (XRD) pattern confirming the crystalline structure of AgNPs.

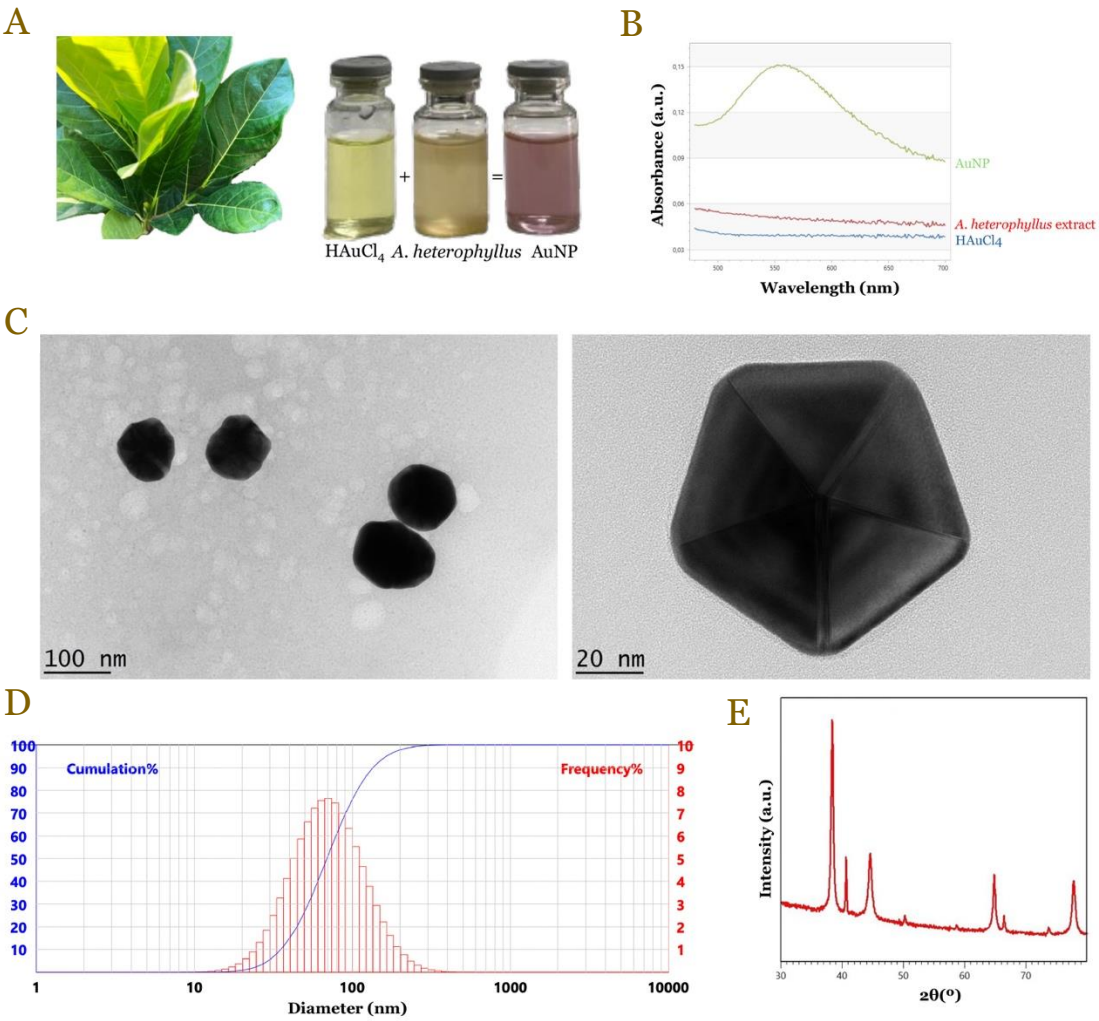

Figure 2. Synthesis and characterization of gold nanoparticles (AuNPs) using *Artocarpus heterophyllus* aqueous leaf extract: (A) The color changes observed during AuNP synthesis; (B) Ultraviolet-visible (UV-Vis) spectroscopic analysis of the synthesized AuNPs; (C) Transmission electron microscopy (TEM) images revealing AuNP morphology; (D) Particle size analysis (PSA) results representing AuNP size distribution; (E) X-ray diffraction (XRD) pattern confirming the crystalline structure of AuNPs.

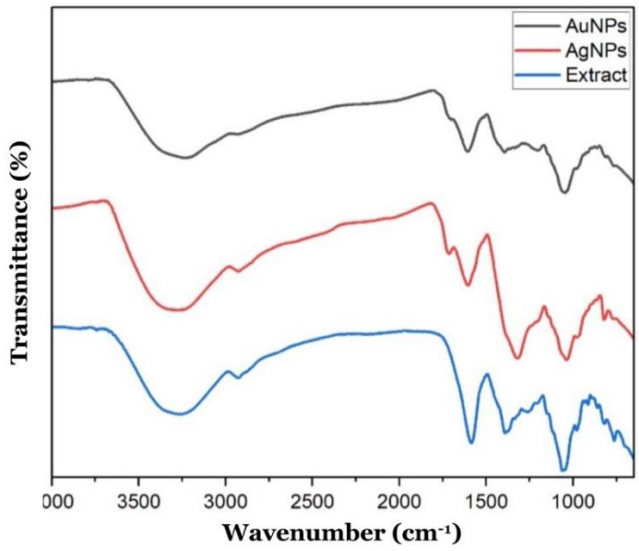

Figure 3. Fourier transform infrared (FT-IR) spectra of *Artocarpus heterophyllus* aqueous leaf extract, silver nanoparticles (AgNPs), and gold nanoparticles (AuNPs).

Anticancer potency of AgNPs and AuNPs from *Artocarpus heterophyllus* aqueous leaf extract

AgNPs had a significant reduction in cell viability at a concentration of 50 µg/mL after 48 hours, with a more pronounced effect observed after 72 hours (**Figure 4A**). In contrast, AuNPs demonstrated cytotoxicity only at higher concentrations (100 and 200 µg/mL) after 48 hours. However, after 72 hours, no significant difference in cell viability was observed between cells treated with the highest AuNP concentration and the control group, suggesting that AuNPs lacked substantial cytotoxic potential against MCF-7 cells (**Figure 4B**). These findings indicated that only AgNPs demonstrated substantial antiproliferative activity against MCF-7 cells, and therefore, further analyses were conducted for AgNPs only.

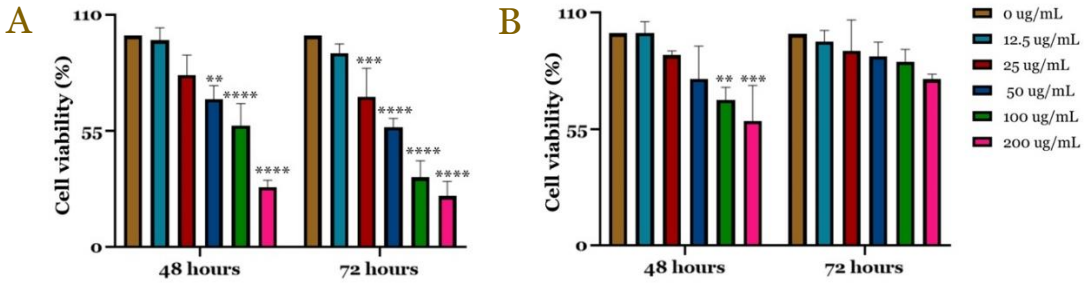

Figure 4. Viability of MCF-7 breast cancer cells following treatment with: (A) silver nanoparticles (AgNPs); and (B) gold nanoparticles (AuNPs) at concentrations of 12.5, 25, 50, 100, and 200 µg/mL for 48 and 72 hours. The asterisk (*) indicates statistically significant differences compared to the negative control group at each respective time point; $^{**}p<0.01$, $^{***}p<0.001$, $^{****}p<0.0001$.

To determine the IC_{50} of AgNPs, a comprehensive analysis was conducted using five concentrations (12.5, 25, 50, 100, and 200 µg/mL) across two incubation periods (48 and 72 hours). AgNPs had potent cytotoxicity, reducing cell viability from 94.32% to 25.01%, with IC_{50} values of 124.62 µg/mL at 48 hours and 54.98 µg/mL at 72 hours (**Figure 5**). These results highlighted the strong antiproliferative effects of AgNPs and their potential application in cancer treatment.

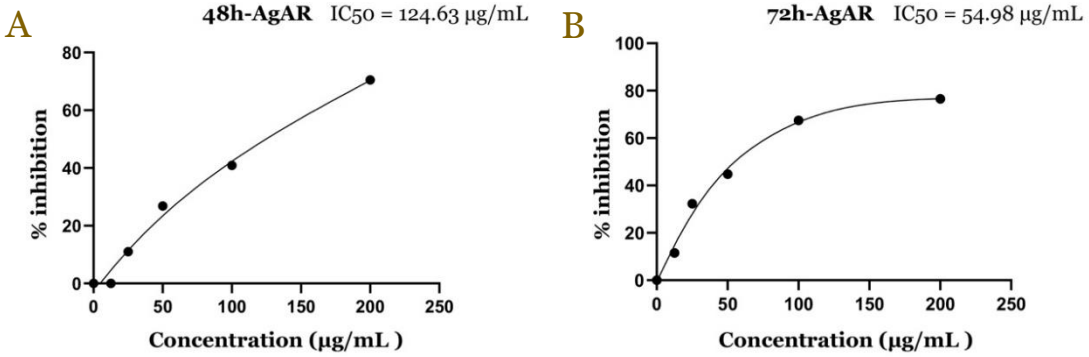

Figure 5. Half-maximal inhibitory concentration (IC_{50}) of silver nanoparticles (AgNPs) synthesized from *Artocarpus heterophyllus* (AR) aqueous leaf extract against the MCF-7 breast cancer cell line after 48 (A) and 72 hours (B) of treatment.

AgNPs derived from *Artocarpus heterophyllus* aqueous leaf extract induced alterations in DNA content, nuclear size, and nuclear area of MCF-7 cells

AgNPs treatment significantly reduced the proportion of cells in the G1 phase (2N DNA content) and the S phase (2N-4N DNA content), while simultaneously increasing the number of cells with DNA content greater than 4N (G2/M phase). This increase in cells with over 4N DNA content may indicate disruptions in chromosome segregation or mitotic processes (**Figure 6A**). Additionally, a significant increase in both nuclear size and nuclear area was observed following AgNPs treatment (**Figure 6B**). These findings demonstrated that AgNPs had their anticancer effects by inducing mitotic dysregulation, leading to genomic instability and potentially triggering an apoptotic pathway in cancer cells.

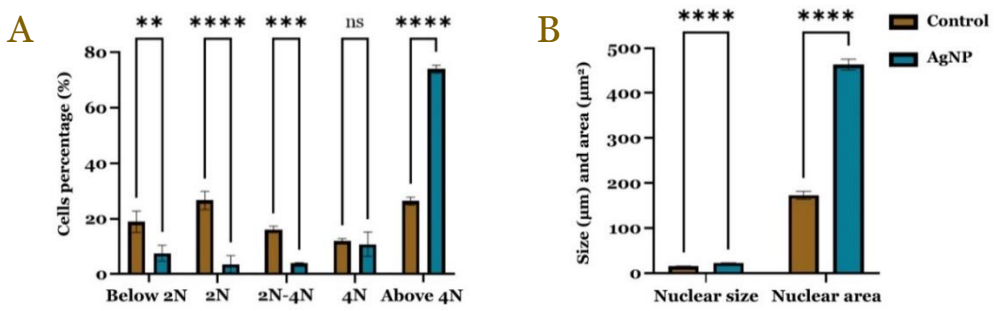

Figure 6. Quantitative analysis of DNA content (A) and nuclear size as well as nuclear area (B) in MCF-7 breast cancer cells following treatment with 50 µg/mL of silver nanoparticles (AgNPs) for 24 hours. The asterisk (*) indicates statistically significant differences compared to the negative control group; $^{**}p<0.01$, $^{***}p<0.001$, $^{****}p<0.0001$.

AgNPs derived from *Artocarpus heterophyllus* aqueous leaf extract modulate the mRNA expression levels of *c-Myc*, *cyclin D1*, *COX-2*, *HER-2*, and *miR-622* in MCF-7 breast cancer cells

Our data indicated that AgNPs derived from *A. heterophyllus* aqueous leaf extract treatment at 200 µg/mL significantly reduced the expression of key oncogenes associated with MCF-7 proliferation and survival (**Figure 7**). The extract significantly reduced the expression of *cyclin D1* (**Figure 7B**), *HER-2* (**Figure 7C**), *miR622* (**Figure 7D**), and *COX-2* (**Figure 7E**) of cMCF-7 cells compared to untreated cells. However, the treatment did not reduce the *c-Myc* expression (**Figure 7A**). These results emphasize the potential of AgNPs in regulating critical oncogenes and provide insights into their mechanisms of anti-proliferative action in cancer cells.

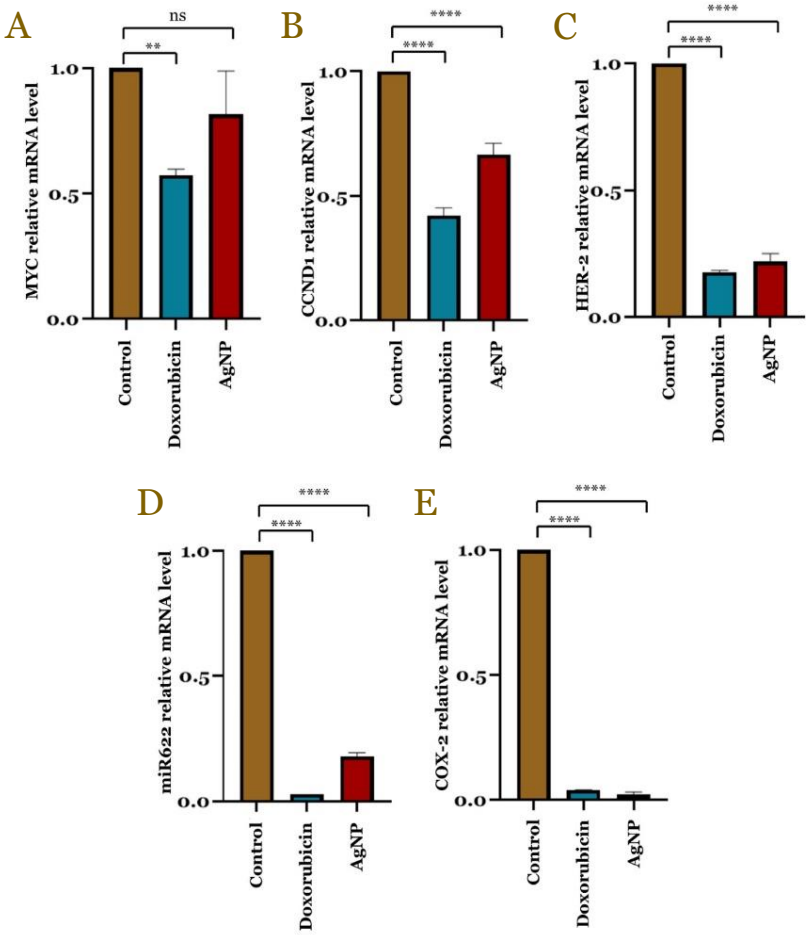

Figure 7. Expression of key oncogenes and tumor-associated genes in MCF-7 breast cancer cells treated with silver nanoparticles (AgNPs): (A) *c-Myc*; (B) *cyclin D1*; (C) *human epidermal growth factor receptor-2* (*HER-2*); (D) *microRNA-622* (*miR-622*); and (E) *cyclooxygenase-2* (*COX-2*). The asterisk (*) indicates statistically significant differences compared to the negative control group; $^{**}p<0.01$, $^{***}p<0.001$, $^{****}p<0.0001$.

Discussion

The characterization of AgNPs and AuNPs synthesized using *A. heterophyllus* aqueous leaf extract is essential for understanding their structural, optical, and biological properties. In the present study, the green synthesis of AgNPs and AuNPs using *A. heterophyllus* leaf extract was conducted, and their potential as anti-breast cancer agents was evaluated. A distinct color change was observed after incubation, with AgNPs turning from beige to dark brown and AuNPs from beige to purplish, confirming the successful formation of nanoparticles via a biological reduction process using the leaf extract, with its phytochemical compounds playing a critical role in the reduction and stabilization of AgNPs and AuNPs. The UV-Vis spectra of AgNPs derived from *A. heterophyllus* aqueous leaf extract showed an absorption peak between 400–440 nm, indicative of nanosilver surface plasmon resonance, with a slight broadening suggesting a polydisperse nature [32,33]. In contrast, AuNPs had a unique absorption spectrum that varied with size, typically peaking between 520–530 nm. As the diameter of AuNPs increased, the peak shifted toward the red end of the spectrum, and absorbance was directly proportional to gold concentration when the size remained constant [34].

The AgNPs synthesized in this study had an average diameter of 12.75 nm, with sizes ranging from 5 to 22 nm. In contrast, AuNPs had an average diameter of 109.26 nm, with particle sizes ranging from 27 to 201 nm. These results differed from previous reports, which indicated that AgNPs synthesized from *A. heterophyllus* were larger, approximately 45 nm [33], while AuNPs were smaller, around 20–25 nm [23]. Such discrepancies may be attributed to variations in the specific parts of *A. heterophyllus* used for synthesis and the methods employed. The difference in particle sizes between AgNPs and AuNPs can be explained by the distinct reduction and stabilization mechanisms mediated by phytochemicals in *A. heterophyllus*. Additionally, gold, with a higher atomic mass and larger atomic radius compared to silver, tends to form larger nanoparticles under similar synthesis conditions [35].

FT-IR analysis provided insights into the functional groups involved in the reduction and stabilization of nanoparticles. The FT-IR spectra from the present study revealed distinct absorption bands corresponding to various organic compounds in the plant extract, including flavonoids, polyphenols, and terpenoids. These compounds played a critical role in reducing metal ions to nanoparticles and stabilizing the resulting particles [15,23,33, 36-38]. Flavonoids, in particular, facilitated metal ion reduction by donating electrons, a process that involved breaking the -O-H bond in the enol form [38]. These flavonoids interacted with metal ions via hydroxyl groups on the catechol structure, which had lower dissociation energy compared to those on the aromatic ring, thus promoting the reduction process [38]. Additionally, flavonoids that oxidized from the enol to keto form during stabilization adhered to the nanoparticle surface, preventing aggregation [38]. The reduction of silver ions (Ag^+ to Ag^0) occurred in AgNPs [36-39], while in AuNPs, the reduction occurred from Au^{3+} to Au^0 [11,14,33]. Differences in the FT-IR spectra of AgNPs and AuNPs, particularly in peak intensity and position, indicated varying affinities of silver and gold ions for specific functional groups. This variation likely resulted in distinct chemical environments for the nanoparticles [40]. Previous studies have also highlighted that differences in FT-IR peaks between AgNPs and AuNPs could be attributed to the chemical environment and interactions with biomolecules present in the synthesis extracts [40-42]. Small shifts in peak positions and the presence of unique peaks suggested that bonding interactions and stabilization mechanisms differed between the two metals [40-42]. Furthermore, the presence of these compounds in the FT-IR spectra indicated their role in contributing to the long-term stability of the nanoparticles by preventing agglomeration [40].

The biological effects of AgNPs and AuNPs were assessed through MTT assays to evaluate cell viability. The results demonstrated that AgNPs and AuNPs synthesized from *A. heterophyllus* aqueous leaf extract had cytotoxic effects on MCF-7 cells, with AgNPs causing a more significant reduction in cell viability compared to AuNPs. The IC_{50} values for AgNPs were 124.62 µg/mL at 48 hours and 54.98 µg/mL at 72 hours. The superior cytotoxicity of AgNPs was attributed to their smaller size and higher reactivity, which likely induced greater oxidative stress within the cells [17]. In contrast, AuNPs, which were relatively inert and larger, demonstrated less cytotoxicity, likely reflecting reduced cellular interaction and uptake [7,17,43]. These findings aligned with

previous research, which indicated that larger AuNPs (60 nm) were less toxic to HK-2 cells compared to smaller variants [44].

Treatment with AgNPs derived from A. heterophyllus aqueous leaf extract significantly influenced both nuclear size and DNA content in cells. Notably, a marked increase in the percentage of cells showing DNA content exceeding 4N was observed after AgNPs treatment. This result suggested that the anticancer effects of AgNPs may be attributed to their ability to induce mitotic catastrophe, a form of cell death occurring during mitosis due to DNA damage or defective spindle assembly. This process can overwhelm the cell's checkpoint mechanisms that normally halt mitotic progression until repairs are made [45]. Eukaryotic cell division relies on multiple pathways to ensure precise genome duplication during each division cycle [46,47]. When these regulatory pathways are disrupted, DNA replication may be reinitiated prematurely, leading to DNA re-replication. This process generates cells with DNA content exceeding 4N, making them highly vulnerable to agents that impair DNA repair mechanisms [48,49]. Thus, selectively inducing DNA re-replication in cancer cells may lead to their elimination without adversely affecting normal cells [48]. Several anticancer compounds exert their effects by inducing mitotic catastrophe, which leads to cell death [50,51]. The findings of the present study highlighted the potential of AgNPs as a selective anticancer agent by elevating DNA content beyond 4N.

The AgNPs significantly altered the mRNA expression of key genes, including *cyclin D1, HER-2, miR-622,* and *COX-2*, which play important roles in regulating cancer cell behavior, such as proliferation, survival, and inflammation [52-55,59,61]. The results indicated that AgNPs treatment significantly downregulated the expression of these genes compared to the control group. *Cyclin D1*, well-known oncogene involved in cell cycle regulation, proliferation, and angiogenesis, was particularly noteworthy, and elevated *cyclin D1* levels are essential for transitioning from the G1 to the S phase in the cell cycle [53]. Cyclin D1 interacts with cyclin-dependent kinases (CDK4 and CDK6), which phosphorylate the retinoblastoma protein, thereby enabling the progression of the cell cycle [52-55].

HER-2, a receptor tyrosine kinase (RTK), is frequently overexpressed in aggressive breast cancers and plays a critical role in regulating cancer stemness and drug resistance [52]. RTKs typically activate PI3K/Akt signaling, promoting the expression of cancer stemness factors and proteins associated with multidrug resistance [52]. The observed suppression of these genes suggested that AgNPs effectively inhibited cancer cell growth and proliferation by targeting these key pathways [56]. The downregulation of *cyclin D1* indicated reduced oncogenic signaling that drives uncontrolled cell division, while the decreased expression of *HER-2* suggested a potential impact on cancer cell survival and metastasis [52-53]. Prior studies have reported that AgNPs could inhibit the proliferation of MCF-7 and DU145 cells by downregulating the *cyclin D1* gene [56,57].

AgNPs also influenced the expression of *COX-2*, a gene associated with inflammation and involved in cancer progression [56]. The significant reduction in *COX-2* expression following AgNP treatment suggested that these nanoparticles might exert anti-inflammatory effects, further inhibiting cancer progression by reducing the inflammatory environment that often supports tumor growth [56,57]. Additionally, *miR-622*, a microRNA implicated in various cancers, regulates the expression of genes associated with cancer cell survival and apoptosis [60-62]. The modulation of *miR-622* by AgNPs indicated that these nanoparticles might influence cancer cell fate through the regulation of miRNA, adding another layer of complexity to their anticancer mechanisms [63].

This study was the first investigation of AgNPs synthesized from *A. heterophyllus* aqueous leaf extract as a potential breast cancer treatment, highlighting their ability to modulate the mRNA expression of key cancer-related genes. This in vitro study demonstrated the anticancer activity of AgNPs synthesized from *A. heterophyllus* aqueous leaf extracts against MCF7 breast cancer cells, offering promising clinical implications. The findings suggested the potential development of a natural, plant-based nanotherapeutic agent for breast cancer treatment, providing a biocompatible and eco-friendly alternative to conventional therapies. The selective activity of AgNPs against cancer cells could facilitate the creation of targeted drug delivery systems, thereby enhancing treatment efficacy while minimizing side effects on healthy tissues. Furthermore, the sustainable and cost-effective synthesis method made this approach

particularly attractive for resource-limited settings, where access to advanced cancer treatments may be limited. By modulating key oncogenic pathways, as shown in the study, these nanoparticles could also complement existing therapies, yielding synergistic effects. Although further in vivo studies and clinical trials are necessary, the research established a solid foundation for the development of innovative and accessible cancer treatments with reduced toxicity and improved efficacy.

While the in vitro study of AgNPs synthesized from aqueous *A. heterophyllus* leaf extracts against MCF-7 cancer cells demonstrated promising anticancer activity, several limitations were identified. Firstly, this in vitro study does not fully replicate the complexity of the human tumor microenvironment, which involves interactions with immune cells, stromal components, and vascular systems. As a result, the observed anticancer effects may not directly translate to in vivo conditions. Additionally, the study did not assess the potential toxicity of AgNPs to normal, healthy cells, a crucial aspect in evaluating the safety profile of the nanoparticles. The long-term stability, bioavailability, and pharmacokinetics of the AgNPs were also not addressed, raising concerns about their practical application in clinical settings. Moreover, the specific molecular mechanisms through which AgNPs exert their anticancer effects require further investigation. These limitations highlight the necessity for comprehensive in vivo studies and preclinical trials to confirm the efficacy, safety, and therapeutic potential of these nanoparticles before advancing to clinical applications.

Future research on AgNPs in vivo should focus on biodistribution, pharmacokinetics, and long-term safety. Understanding how these nanoparticles accumulate in tissues is essential for assessing their therapeutic potential and safety. Pharmacokinetic studies should clarify their absorption, metabolism, and excretion, which are crucial for effective dosing. Long-term safety assessments should identify any chronic effects resulting from prolonged exposure. However, translating this technology to clinical use presents several challenges, including regulatory hurdles, ensuring consistent manufacturing, and addressing patient-specific responses. Additionally, managing public perception and ethical concerns is necessary to gain acceptance of nanoparticle therapies. A collaborative effort among researchers, clinicians, and regulatory bodies is crucial to overcome these obstacles and maximize the benefits of AgNPs in medicine.

Conclusion

AgNPs and AuNPs synthesized using *A. heterophyllus* aqueous leaf extract had distinct shapes and sizes. The AgNPs averaged approximately 12.75 nm in size and were spherical, whereas the AuNPs had an average size of 109.26 nm and displayed a pentagonal shape. Interestingly, the synthesized AgNPs demonstrated greater efficacy against MCF-7 cell lines, while the AuNPs showed negligible effects. The anticancer efficacy of AgNPs was attributed to the ability to induce mitotic catastrophe, leading to apoptotic cell death. Additionally, AgNPs may exert anticancer effects by downregulating the expression of several oncogenes (*cyclin D1, HER2, miR622*, and *COX-2*) that play vital roles in regulating cancer cell behavior, including proliferation, survival, and inflammation.

Ethics approval

Not required.

Acknowledgments

The authors acknowledge the facilities, scientific and technical support from In Vitro Imaging Laboratory of National Research and Innovation Agency Republic of Indonesia, Bogor, Indonesia.

Competing interests

All the authors declare that there are no conflicts of interest.

Funding

This study was supported by the DRTPM of the Ministry of Education, Culture, Research, and Technology of the Republic of Indonesia, through the Hibah Fundamental Reguler Program

(Grant number: 1734/B/UN3.LPPM/PT.01.03/2024) and the funding from the University of Malaya (Grant number: IF033-2024).

Underlying data

The data supporting the findings of this study are available from the corresponding author upon request.

Declaration of artificial intelligence use

This study used artificial intelligence (AI) tool and methodology, of which AI-based language model ChatGPT was employed in the language refinement (improving grammar, sentence structure, and readability of the manuscript). We confirm that all AI-assisted processes were critically reviewed by the authors to ensure the integrity and reliability of the results. The final decisions and interpretations presented in this article were solely made by the authors.

How to cite

Dewi FRP, Rohmatika AU, Jamil AKM, *et al*. Plant-based synthesis of gold and silver nanoparticles using *Artocarpus heterophyllus* aqueous leaf extract and its anticancer potency. Narra J 2025; 5 (2): e1770 - http://doi.org/10.52225/narra.v5i2.1770.

References

1. Barrios CH. Global challenges in breast cancer detection and treatment. Breast 2022;62 Suppl 1(Suppl 1):S3-S6.
2. Bhushan A, Gonsalves A, Menon JU. Current state of breast cancer diagnosis, treatment, and theranostics. Pharmaceutics 2021;13(5):723.
3. Malik JA, Ahmed S, Jan B, *et al*. Drugs repurposed: An advanced step towards the treatment of breast cancer and associated challenges. Biomed Pharmacother 2022;145:112375.
4. Chehelgerdi M, Chehelgerdi M, Allela OQB, *et al*. Progressing nanotechnology to improve targeted cancer treatment: Overcoming hurdles in its clinical implementation. Mol Cancer 2023;22(1):169.
5. Dewi FRP, Lim V, Rosyidah A, *et al*. Characterization of silver nanoparticles (AgNPs) synthesized from *Piper ornatum* leaf extract and its activity against food borne pathogen *Staphylococcus aureus*. Biodiversitas 2023;24(3):1742-1748.
6. Talarska P, Boruczkowski M, Zurawski J. Current knowledge of silver and gold nanoparticles in laboratory research-application, toxicity, cellular uptake. Nanomaterials (Basel) 2021;11(9):2454.
7. Xu M, Han X, Xiong H, *et al*. Cancer nanomedicine: Emerging strategies and therapeutic potentials. Molecules 2023;28(13):5145.
8. Luo LJ, Lin TY, Yao CH, *et al*. Dual-functional gelatin-capped silver nanoparticles for antibacterial and antiangiogenic treatment of bacterial keratitis. J Colloid Interface Sci 2019;536:112-126.
9. Onitsuka S, Hamada T, Okamura H. Preparation of antimicrobial gold and silver nanoparticles from tea leaf extracts. Colloids Surf B Biointerfaces 2019;173:242-248.
10. Singh P, Ahn S, Kang JP, *et al*. In vitro anti-inflammatory activity of spherical silver nanoparticles and monodisperse hexagonal gold nanoparticles by fruit extract of *Prunus serrulata*: A green synthetic approach. Artif Cells Nanomed Biotechnol 2018;46(8):2022-2032.
11. Tiloke C, Phulukdaree A, Anand K, *et al*. *Moringa oleifera* gold nanoparticles modulate oncogenes, tumor suppressor genes, and caspase-9 splice variants in A549 cells. J Cell Biochem 2016;117(10):2302-2314.
12. Vijayan R, Joseph S, Mathew B. Anticancer, antimicrobial, antioxidant, and catalytic activities of green-synthesized silver and gold nanoparticles using *Bauhinia purpurea* leaf extract. Bioprocess Biosyst Eng 2019;42(2):305-319.
13. Modan EM, Plăiaşu AG. Advantages and disadvantages of chemical methods in the elaboration of nanomaterials. Ann "Dunarea de Jos" Univ Galati Fascicle IX Metall Mater Sci 2020;43(1):53-60.
14. Radulescu DM, Surdu VA, Ficai A, *et al*. Green synthesis of metal and metal oxide nanoparticles: A review of the principles and biomedical applications. Int J Mol Sci 2023;24(20):15397.
15. Berta L, Coman NA, Rusu A, *et al*. A review on plant-mediated synthesis of bimetallic nanoparticles, characterisation and their biological applications. Materials (Basel) 2021;14(24):7677.
16. Muddapur UM, Alshehri S, Ghoneim MM, *et al*. Plant-based synthesis of gold nanoparticles and theranostic applications: A review. Molecules 2022;27(4):1391.

17. Osman AI, Zhang Y, Farghali M, *et al*. Synthesis of green nanoparticles for energy, biomedical, environmental, agricultural, and food applications: A review. Environ Chem Lett 2024;22(2):841-887.
18. Kulkarni D, Sherkar R, Shirsathe C, *et al*. Biofabrication of nanoparticles: Sources, synthesis, and biomedical applications. Front Bioeng Biotechnol 2023;11:1159193.
19. Bidian C, Filip GA, David L, *et al*. Green synthesized gold and silver nanoparticles increased oxidative stress and induced cell death in colorectal adenocarcinoma cells. Nanomaterials (Basel) 2023;13(7):1251.
20. Gupta AK, Rather MA, Kumar Jha A, *et al*. *Artocarpus lakoocha* Roxb. and *Artocarpus heterophyllus* Lam. flowers: New sources of bioactive compounds. Plants (Basel) 2020;9(10):1329.
21. Morrison IJ, Zhang J, Lin J, *et al*. Potential chemopreventive, anticancer and anti-inflammatory properties of a refined artocarpin-rich wood extract of *Artocarpus heterophyllus* Lam. Sci Rep 2021;11(1):6854.
22. Septama AW, Daud NNNNM. Artocarpanone isolated from *Artocarpus heterophyllus* heartwoods enhances cytotoxic effect of cisplatin against H460 and MCF-7 cell lines. IOP Conf Ser Mater Sci Eng 2021;1011(1):012015.
23. Basavegowda N, Dhanya Kumar G, Tyliszczak B, *et al*. One-step synthesis of highly-biocompatible spherical gold nanoparticles using *Artocarpus heterophyllus* Lam. (jackfruit) fruit extract and its effect on pathogens. Ann Agric Environ Med 2015;22(1):84-89.
24. Manikandan V, Yi P, Velmurugan P, *et al*. Production, optimization and characterization of silver oxide nanoparticles using *Artocarpus heterophyllus* rind extract and their antifungal activity. Afr J Biotechnol 2017;16(36):1819-1825.
25. Rodrigues JFB, Azevedo VS, Medeiros RP, *et al*. Physicochemical, morphological, and cytotoxic properties of Brazilian jackfruit (*Artocarpus heterophyllus*) starch scaffold loaded with silver nanoparticles. J Funct Biomater 2023;14(3):143.
26. Tang P, Shen Y, Yang J, *et al*. miR-622 induces breast cancer cell MCF-7 proliferation, migration, and invasion by directly negatively targeting EYA1. J Nanomater 2022;2022:9000689.
27. Nisa N, Wahyuningsih SPA, Darmanto W, *et al*. Effect of the ethanol extract of red okra pods (*Abelmoschus esculentus* (L.) Moench) to inhibit cervical cancer cells growth through cell cycle-associated oncogenes. Scientifica (Cairo) 2022;2022:1094771.
28. Dewi FRP, Wahyuningsih SPA, Tan SC, *et al*. Green synthesis of gold nanoparticles from *Stachytarpheta jamaicensis*: An eco-friendly approach with promising anticancer potency. Nanomedicine J 2025;12(1):51-58.
29. Cao GD, Chen K, Chen B, *et al*. Positive prognostic value of HER2-HER3 co-expression and p-mTOR in gastric cancer patients. BMC Cancer 2017;17(1):841.
30. Roelofs HMJ, te Morsche RHM, van Heumen BWH, *et al*. Over-expression of COX-2 mRNA in colorectal cancer. BMC Gastroenterol 2014;14:1.
31. Huang W, Wang L, Long D, *et al*. Colorimetric determination and recycling of gold(III) ions using label-free plasmonic $H_{0.3}MoO_3$ nanoparticles. Mikrochim Acta 2023;190(6):245.
32. Ashraf JM, Ansari MA, Khan HM, *et al*. Green synthesis of silver nanoparticles and characterization of their inhibitory effects on AGEs formation using biophysical techniques. Sci Rep 2016;6:20414.
33. Manjare SB, Gurav VL, Chavan R, *et al*. Silver Nanoparticles synthesis using AH leaf extract and its antimicrobial activity. Bioinspired Biomim Nanobiomaterials 2020;9(3):190-193.
34. He YQ, Liu SP, Kong L, *et al*. A study on the sizes and concentrations of gold nanoparticles by spectra of absorption, resonance Rayleigh scattering and resonance non-linear scattering. Spectrochim Acta A Mol Biomol Spectrosc 2005;61(13-14):2861-2866.
35. Solati E, Dorranian D. Comparison between silver and gold nanoparticles prepared by pulsed laser ablation in distilled water. J Clust Sci 2015;26:727-742.
36. Habeeb Rahuman HB, Dhandapani R, Narayanan S, *et al*. Medicinal plants mediated the green synthesis of silver nanoparticles and their biomedical applications. IET Nanobiotechnol 2022;16(4):115-144.
37. Jain AS, Pawar PS, Sarkar A, *et al*. Bionanofactories for green synthesis of silver nanoparticles: Toward antimicrobial applications. Int J Mol Sci 2021;22(21):11993.
38. Zuhrotun A, Oktaviani DJ, Hasanah AN. Biosynthesis of gold and silver nanoparticles using phytochemical compounds. Molecules 2023;28(7):3240.
39. Sharma NK, Vishwakarma J, Rai S, *et al*. Green route synthesis and characterization techniques of silver nanoparticles and their biological adeptness. ACS Omega 2022;7(31):27004-27020.
40. Nayem SMA, Sultana N, Haque MA, *et al*. Green synthesis of gold and silver nanoparticles by using *Amorphophallus paeoniifolius* tuber extract and evaluation of their antibacterial activity. Molecules 2020;25(20):4773.
41. Foti A, Cali L, Petralia S, *et al*. Green nanoformulations of polyvinylpyrrolidone-capped metal nanoparticles: A study at the hybrid interface with biomimetic cell membranes and in vitro cell models. Nanomaterials (Basel) 2023;13(10):1624.

42. Velmurugan P, Lee SM, Cho M, *et al*. Antibacterial activity of silver nanoparticle-coated fabric and leather against odor and skin infection causing bacteria. Appl Microbiol Biotechnol 2014;98(19):8179-8189.
43. Niznik L, Noga M, Kobylarz D, *et al*. Gold nanoparticles (AuNPs)-toxicity, safety and green synthesis: A critical review. Int J Mol Sci 2024;25(7):4057.
44. Enea M, Pereira E, de Almeida MP, *et al*. Gold nanoparticles induce oxidative stress and apoptosis in human kidney cells. Nanomaterials (Basel) 2020;10(5):995.
45. Castedo M, Perfettini JL, Roumier T, *et al*. Cell death by mitotic catastrophe: A molecular definition. Oncogene 2004;23(16):2825-2837.
46. DePamphilis ML, Blow JJ, Ghosh S, *et al*. Regulating the licensing of DNA replication origins in metazoa. Curr Opin Cell Biol 2006;18(3):231-239.
47. Blow JJ, Gillespie PJ. Replication licensing and cancer: A fatal entanglement? Nat Rev Cancer 2008;8(10):799-806.
48. Zhu W, Dutta A. An ATR- and BRCA1-mediated Fanconi anemia pathway is required for activating the G2/M checkpoint and DNA damage repair upon rereplication. Mol Cell Biol 2006;26(12):4601-4611.
49. Melixetian M, Ballabeni A, Masiero L, *et al*. Loss of Geminin induces rereplication in the presence of functional p53. J Cell Biol 2004;165(4):473-482.
50. Dewi FRP, Domoto T, Hazawa M, *et al*. Colorectal cancer cells require glycogen synthase kinase-3beta for sustaining mitosis via translocated promoter region (TPR)-dynein interaction. Oncotarget 2018;9(17):13337-13352.
51. Yoshino Y, Ishioka C. Inhibition of glycogen synthase kinase-3 beta induces apoptosis and mitotic catastrophe by disrupting centrosome regulation in cancer cells. Sci Rep 2015;5:13249.
52. Feng Y, Spezia M, Huang S, *et al*. Breast cancer development and progression: Risk factors, cancer stem cells, signaling pathways, genomics, and molecular pathogenesis. Genes Dis 2018;5(2):77-106.
53. Gao FY, Li XT, Xu K, *et al*. c-MYC mediates the crosstalk between breast cancer cells and tumor microenvironment. Cell Commun Signal 2023;21(1):28.
54. Lundberg A, Lindstrom LS, Li J, *et al*. The long-term prognostic and predictive capacity of cyclin D1 gene amplification in 2305 breast tumours. Breast Cancer Res 2019;21(1):34.
55. Wang C, Zhang J, Yin J, *et al*. Alternative approaches to target Myc for cancer treatment. Signal Transduct Target Ther 2021;6(1):117.
56. Gandhi AD, Miraclin PA, Abilash D, *et al*. Nanosilver reinforced *Parmelia sulcata* extract efficiently induces apoptosis and inhibits proliferative signalling in MCF-7 cells. Environ Res 2021;199:111375.
57. Singh SP, Mishra A, Shyanti RK, *et al*. Silver nanoparticles synthesized using *Carica papaya* leaf extract (AgNPs-PLE) causes cell cycle arrest and apoptosis in human prostate (DU145) cancer cells. Biol Trace Elem Res 2021;199(4):1316-1331.
58. Gandhi J, Khera L, Gaur N, *et al*. Role of modulator of inflammation cyclooxygenase-2 in gammaherpesvirus mediated tumorigenesis. Front Microbiol 2017;8:538.
59. Liu B, Qu L, Yan S. Cyclooxygenase-2 promotes tumor growth and suppresses tumor immunity. Cancer Cell Int 2015;15:106.
60. Cheng CW, Liu YF, Liao WL, *et al*. miR-622 increases miR-30a expression through inhibition of hypoxia-inducible factor 1α to improve metastasis and chemoresistance in human invasive breast cancer cells. Cancers (Basel) 2024;16(3):657.
61. Lu J, Xie Z, Xiao Z, *et al*. The expression and function of miR-622 in a variety of tumors. Biomed Pharmacother 2022;146:112544.
62. Peng Y, Croce CM. The role of microRNAs in human cancer. Signal Transduct Target Ther 2016;1:15004.
63. Wang B, Hu S, Teng Y, *et al*. Current advance of nanotechnology in diagnosis and treatment for malignant tumors. Signal Transduct Target Ther 2024;9(1):200.